

1 We want to thank Matthias Konrad-Schmolke for his critical review and suggestions. Below is a list of
2 all comments from the reviewer (RC), answers from the authors (AC) and manuscript changes (MC).

3

4 **Reviewer 1, general comment**

5 **RC:** One crucial argument for crystal plasticity in garnet is the observation of dislocation walls that
6 mark the boundary of one subgrain in the garnet crystals. The authors state that these dislocation
7 walls are the result of dislocation climb in the crystal (lines 252-253) and therefore indicate the
8 activity of viscous deformation mechanisms in garnet. I am not entirely convinced that these
9 dislocation walls are only produced by the migration of dislocations through the crystal, although I
10 am not aware of studies that demonstrate neither pro nor contra arguments. The fact that the
11 authors do not cite any references is also not helpful with this regard. However, there is evidence
12 that such dislocation walls can be generated in undeformed rocks, e.g. during fluid infiltration, such
13 as demonstrated in Konrad-Schmolke et al., 2018. Of course, fluid infiltration does not play a role in
14 the rocks presented here, but other mechanisms for the formation of the dislocation walls must be
15 discussed in this manuscript, as these structures are a fundamental argument for crystal plasticity.
16 Furthermore, the interpretation of the presence of rotated subgrains in terms of subgrain rotation
17 recrystallization is, in my opinion, also questionable. Konrad-Schmolke et al., 2007 demonstrate the
18 presence of subgrains in garnets (and their slight misorientations) in undeformed rocks. In general, I
19 think that the manuscript would very much benefit from a more indepth discussion of these
20 features. The papers cited in this review should only serve as examples and I think that there are
21 many other contributions to the topic that I am not aware of at the moment. However, I think the
22 manuscript is very well suitable for publication after moderate revisions and a more thorough
23 discussion.

24 **AC:** As noted by the reviewer, fluid infiltration does not play a role in the rocks presented here, so
25 the mechanism proposed in Konrad-Schmolke et al., 2018 cannot be relevant in this case. The rocks
26 we are considering here are also clearly deformed, with stresses being high enough (at least
27 transiently) to cause fracturing of garnet. Progressive subgrain rotation by migration of dislocations
28 into walls bounding such subgrains is a mechanism that has been very widely proposed both in the
29 material and earth sciences. There is a large body of published work supporting and describing this
30 mechanism – indeed as noted by the reviewer “I think that there are many other contributions to
31 the topic”. It is not the aim of the current manuscript to provide an exhaustive review be we have
32 now added the following additional references as a representative selection:

33 Hobbs, B.E.: Recrystallisation of single crystals of quartz. *Tectonophysics*, 6, 353-401, 1968.

34 Passchier, C.W., Trouw, R.A.J.: *Microtectonics* (2nd Edition), Springer, Heidelberg, 366 pp., 2005.

35

36 **Reviewer 1, specific comments**

37 **RC:** Line 138: if the fractures a dilatant there must be some material in the cracks. Can that be
38 evaluated?

39 **AC:** No, these fractures remain empty, as implied by the word “unfilled” in the original text. These
40 fractures are Mode 1 extensional fractures, which we think open during propagation of the seismic
41 wave and immediately close, preventing any mineral filling.

MC: The word “dilatant” is perhaps better replaced with “extensional”, so the text now reads “An apparent late generation of unfilled extensional fractures [...]”. All other similar references to “dilatant fractures” have also now been changed to “extensional fractures”.

RC: What about the other, fast diffusing elements, such as Mn and Mg? Differences in diffusion lengths would indicate different diffusion velocities and thus support the idea of a diffusional modification.

AC: In Figure 4 d) we present the profiles for Fe, Mg, Mn. Fe and Mg show the same diffusion length as Ca. Mn does not show any measurable modification throughout the crystal.

MC: This observation was missing in the text, therefore we added the following sentence for clarification: “The length-scale for variation in Fe (X_{Alm}) and Mg (X_{Pyx}) is identical to that for Ca (X_{Grs}), whereas the Mn content (X_{SpS}) does not show any variation (Fig 4d).”

RC: Lines 196-197: This diffusional modification is likely due to subgrain boundaries that might or might not be associated with subgrain rotations. This has been demonstrated in Konrad-Schmolke et al., 2007 (EJM). This should be discussed or at least mentioned.

AC: Since a subgrain is defined by a relative crystallographic rotation (commonly taken arbitrarily as between ca. 4° and 15°, when it is considered to be a “high-angle boundary” to a “new grain”, e.g. Urai et al., 1986), the generally accepted argument is that subgrain boundaries are always associated with subgrain rotations, as new dislocations are continuously added to the subgrain boundaries (e.g. Passchier and Trouw, 2005, p.43). We have added the reference to Konrad-Schmolke et al. (2007), as well as recent publications of Petley-Ragan et al. (2019), Jamtveit et al. (2018a,b, in press), Engi et al. (2018), Giuntoli et al. (2018) and Angiboust et al. (2017) when comparing and contrasting our “dry” results to fracture and diffusion in garnets in deep-seated rocks where fluid infiltration plays an important role.

We want to thank the anonymous reviewer for his critical review and suggestions. Below is a list of all comments from the reviewer (RC), answers from the authors (AC) and manuscript changes (MC).

Reviewer 2, general comment

RC: The main message of this manuscript is the occurrence of crystal plasticity in garnet at temperatures well below the laboratory derived data for the onset of crystal plastic deformation in garnet. The authors, therefore, state that laboratory data fail to explain the natural observations. Of course laboratory experiments are most often very simplified rendering extrapolation to natural systems rather challenging. Though, I miss a bit the explanation why the laboratory data does not match natural observations. Is it because the samples in the laboratory were even drier than the natural rock delaying the onset of crystal plastic deformation in the laboratory? Obviously there were some fluids present due to the occurrence of biotite. Though in some parts of the manuscript, the authors state that a Ca-rich garnet forms instead of epidote, because of the low water activity (line 290). Perhaps there was enough water around to facilitate crystal plastic deformation but not

83 enough to stabilize epidote? I think it would improve the manuscript to discuss the role of fluids on
 84 crystal plastic deformation in more detail. This might also explain the discrepancy between
 85 laboratory data and the natural observations.

86 **AC:** We have added text in several places to expand the discussion of the apparent discrepancy with
 87 laboratory data, in particular considering the potential effects of strain rate and role of fluids. We
 88 agree that this should have been treated in more detail, which is why we now have a rather more
 89 nuanced approach, considering factors that may have an influence rather than just stating that there
 90 is a difference.

91

92 **RC:** Line 71: In this context I think crystal plastic deformation instead of ductile deformation is more
 93 appropriate.

94 **AC:** agree

95 **MC:** changed sentence: “*between brittle and crystal plastic deformation of garnet*”

96

97 **RC:** Lines 276-278: Did you investigate/find garnet crystals that were cut by a pseudotachylyte? Both
 98 studies that you cite, Austrheim et al. (2017) and Papa et al. (2018), demonstrate garnet crystals that
 99 are situated right next to a pseudotachylyte-bearing fault. I mention this, because as strain rate and
 100 stresses decrease very rapidly with increasing distance, the required stresses and/or strain rates at a
 101 few mm to the fault might not be sufficient anymore to extensively fragment garnet.

102 **AC:** In the text, we clearly state that “*Granulite facies garnet porphyroclasts in Musgravian*
 103 *peraluminous gneisses mylonitized during the Petermann Orogeny are almost invariably fractured,*
 104 *irrespective of their proximity to pseudotachylyte (Fig. 3).*” This is different than what was observed
 105 in the examples of Austrheim et al. (2017) and Papa et al. (2018) mentioned above, which is why we
 106 made such a clear statement originally. On the basis of this observation, we argue in the text that
 107 the whole rock was affected by high stresses during transient seismic events and that garnet
 108 fracturing is not restricted to the localized damage zone of a propagating fracture (Petley-Ragan et
 109 al, 2019; Austrheim et al., 2017) or thermal shock immediately adjacent to the high temperature
 110 pseudotachylyte (Papa et al., 2018).

111

112 **RC:** Line 286: Delete ‘of some’.

113 **AC:** agree

114 **MC:** Typing error corrected.

115

116 **RC:** Lines 291-292: So everything is dry, but suddenly there is biotite? You should discuss the
 117 presence/absence of hydrous minerals a bit more.

118 **AC:** Biotite is a typical mineral of granulite facies assemblages up to the point of melting (with biotite
 119 then providing the water for “anhydrous” melting) and even then biotite is a common mineral in the
 120 restite assemblage. “Kinzigite”, which is a typical “dry” lower-crustal granulite facies rock, is actually
 121 defined as having garnet + biotite. As noted by Pennacchioni and Cesare (1997), under upper

122 amphibolite facies conditions, newly grown biotite can actually act as a sink for any free water
 123 available and the same will be true for the “dry” high pressure upper amphibolite (“sub-eclogitic”)
 124 facies conditions relevant to the current study.

125 Pennacchioni, G. & Cesare, B., 1997. Ductile-brittle transition in pre-Alpine amphibolite facies
 126 mylonites during evolution from water-present to water-deficient conditions (Mont Mary nappe,
 127 Italian Western Alps). Jour. Metm. Geol. 15, 777-791.

128

129 **RC:** Lines 304-305: Shimada et al. (1983) experimentally investigated that the angle changes from
 130 around 30 to approx. 45° with increasing pressure.

131 **MC:** The reference was added to the text: *“This plot is only qualitative, since the angle of internal*
 132 *friction could decrease towards higher pressure (Shimada et al., 1983).”*

133

134 **RC:** Lines 311-313: See comment above. As water seems important you should perhaps quantify the
 135 amount of water? There is some water present in the other field studies mentioned, but not very
 136 much. How should the presence of a fluid help to fragment the rock?

137 **AC:** As noted already in Wex et al. (2018), for the relevant pressure and temperature conditions, the
 138 presence of kyanite as the result of plagioclase breakdown, to the exclusion of clinozoisite / epidote,
 139 implies a water activity of less than ca. 0.004, according to Wayte et al. (1989) (as is also noted again
 140 in the current manuscript). The examples from Holsnoy all have extensive development of
 141 clinozoisite during eclogite formation.

142

143 **RC:** Figure 5: The difference between fracture types I and II is not very clear to me. The magnification
 144 at which the image was taken is quite low and therefore it is difficult to see subgrains.

145 **AC:** The step-size for this map was 2 micrometres, which is obviously a compromise due to the large
 146 area of the garnet, and individual points are still visible in the figure. Unfortunately, we do not have
 147 a higher resolution scan for the specific area. We hope that the subgrains are still visible as slight
 148 changes in colour and grey-values, as seen and highlighted in the red area. We admit that there is no
 149 genetic difference between the proposed fracture sets I and II and have therefore dropped any
 150 differentiation between the two.

151 **MC:** Figure 5 was changed in regard to the labelling of the fractures and the text was changed
 152 accordingly.

153

154

155

156 **MANUSCRIPT INCLUDING CHANGES**

157 **Fracturing and crystal plastic behaviour of garnet under seismic stress in the**
158 **dry lower continental crust (Musgrave Ranges, Central Australia)**

159

160

161 Friedrich Hawemann^{1*}, Neil Mancktelow¹, Sebastian Wex¹, Giorgio Pennacchioni², Alfredo
162 Camacho³

163 1) Department of Earth Sciences, ETH Zurich, CH8092 Zurich, Switzerland

164 2) Department of Geosciences, University of Padova, Padova, Italy

165 3) Department of Geological Sciences, University of Manitoba, Winnipeg, Manitoba, R3T
166 2N2, Canada

167 * corresponding author friedrich.hawemann@erdw.ethz.ch

168

169 **Highlights**

- 170 • garnet deformed by fracturing and crystal-plasticity under dry lower crustal conditions
- 171 • Ca-diffusion profiles indicate multiple generations of fracturing
- 172 • diffusion is promoted along zones of higher dislocation density
- 173 • fracturing indicates transient high-stress (seismic) events in the lower continental
- 174 crust

175 **Abstract**

176 Garnet is a high strength mineral compared to other common minerals such as quartz and
177 feldspar in the felsic crust. In felsic mylonites, garnet typically occurs as porphyroclasts that
178 mostly evade intracrystalline crystal-plastic deformation, except under relatively high
179 temperature conditions. The microstructure of granulite facies garnet in felsic lower-crustal
180 rocks of the Musgrave Ranges (Central Australia) records both fracturing and crystal-plastic
181 deformation. Granulite facies metamorphism at ~ 1200 Ma generally dehydrated the rocks
182 and produced mm-sized garnets in peraluminous gneisses. A later ~ 550 Ma overprint under
183 sub-eclogitic conditions (600-700 °C, 1.1-1.3 GPa) developed mylonitic shear zones and with
184 abundant pseudotachylyte, coeval with the neocrystallization of fine-grained, high-calcium
185 garnet. In the mylonites, The granulite facies fractured garnet porphyroclasts in mylonites
186 show have high are enriched in calcium content along rims and fractures. However, in certain
187 cases, these rims are locally narrower than equivalent otherwise comparable rims along
188 original grain boundaries, indicating contemporaneous diffusion and fracturing of garnet. The
189 fractured garnets exhibit internal crystal-plastic deformation, that which coincides with areas
190 of enhanced diffusion, usually along zones of crystal lattice distortions and dislocation walls
191 and by associated with subgrain rotation recrystallization. Fracturing of garnet under dry
192 lower crustal conditions, in an otherwise viscously flowing matrix, requires transient high
193 differential stress, most likely related to seismic rupture, consistent with the coeval
194 development of abundant pseudotachylyte.

195

196 **Keywords**

197 Garnet, Fracture, Crystal-Plasticity, Dry Lower Continental Crust, Pseudotachylyte, Seismicity

1 Introduction

A fundamental problem in geology is the limited preservation of processes in the rock record. This is especially the case for transient events, like earthquakes, traces of which are hardly preserved due to later reworking. The best indicators for seismicity in the rock record are pseudotachylytes (Sibson, 1975; Toy et al., 2011), although not every seismic event produces frictional melts and, once formed, ductile creep or later brittle fracturing may erase most traces (Sibson and Toy, 2006; Kirkpatrick and Rowe, 2013).

Garnet is stable in many metamorphic rocks over a large part of the pressure-temperature space, is commonly preserved, and is suitable for a range of geothermobarometers and geochronometers and their combination for geospeedometry (Lasaga, 1983; Caddick et al., 2010; Baxter and Scherer, 2013). Being a high strength mineral (Karato et al., 1995; Wang and Ji, 1999), both brittle and crystal plastic deformation are rarely observed in garnet when compared to the common matrix minerals of the crust, such as quartz and feldspar. However, Dalziel and Bailey (1968) already interpreted elongate garnets in a high grade mylonites as to be the result of crystal plastic behavior/behaviour – and Advancements/advancements since then in electron microscopy, and especially EBSD (electron backscatter diffraction), have allowed detailed investigation of garnet textures (Kunze et al., 1993; Prior et al., 2000, 2002).

Experimental deformation of garnet indicates that differential stresses on the order of a few GPa are required to produce shear fractures (Wang and Ji, 1999), and that the onset of ductile crystal plastic behavior/behaviour for strain rates typical of actively deforming regions (10^{-12} – 10^{-15} s⁻¹; e.g. Behr and Platt, 2011) should only occur at corresponding temperatures above ca. 750-640 850 °C (Karato et al., 1995; Wang and Ji, 1999). The observation of fractured garnets in natural samples may therefore be linked to seismic stresses, as suggested by

221 Austrheim et al. (1996), who described fracturing of garnets during pseudotachylyte
 222 formation and fluid-assisted eclogitization of granulites. Trepmann and Stöckhert (2002) also
 223 interpreted the microstructure of fractured and offset garnets as evidence for syn-seismic
 224 loading and post-seismic creep. ~~In addition, and, m. More recently, Austrheim et al. (2017)~~
 225 ~~again also associated both~~ brittle (Austrheim et al., 2017; Engi et al., 2017; Angiboust et al.,
 226 2017; Giuntoli et al., 2018; Hawemann et al., 2018; Petley-Ragan et al., 2019) and associated
 227 crystal-plastic ~~behavior~~ behaviour (Austrheim et al., 2017; Petley-Ragan et al., 2019) of garnets
 228 ~~has been related to with lower crustal~~ seismic events in lower continental crust or deeply
 229 ~~subducted continental fragments~~. Papa et al. (2018) interpreted similar deep-seated dilatant
 230 fracturing of garnet immediately adjacent to pseudotachylyte to be related to thermal shock
 231 due to frictional heating rather than to damage associated with propagation of the seismic
 232 rupture. ~~Konrad-Schmolke et al. (2007) described enhanced diffusion of Mg along subgrain~~
 233 ~~boundaries in garnet (but not of slow diffusing elements, such as Ca, Ti and Y) from meta-~~
 234 ~~granitoid-high pressure meta-granitoid rocks of the deeply subducted Sesia Zone (Western~~
 235 ~~Alps).- However, in contrast to more recent studies in the Sesia Zone, which propose that~~
 236 ~~precursor fracturing was crucial for dissolution-precipitation and diffusion processes in~~
 237 ~~garnet (Engi et al., 2018; Giuntoli et al., 2018), they considered that there were no signs of~~
 238 ~~crystal-plastic deformation in their garnet samples and concluded that a diffusion-induced~~
 239 ~~dislocation migration and/or diffusion-induced recrystallisation process was responsible for~~
 240 ~~development of the observed subgrain texture.~~
 241 Here we present a study of garnet microstructures from lower crustal rocks of the Musgrave
 242 Block in Australia, which:

- (1) illustrates the close association between brittle and ~~ductile—crystal—plastic~~ deformation of garnet under well-established pressure-temperature conditions;
- (2) infers deformation mechanisms from the observed microstructure;
- (3) explores the close link between deformation and diffusion in garnet;
- (4) complements other independent observations indicating transient high stresses in the lower crust.

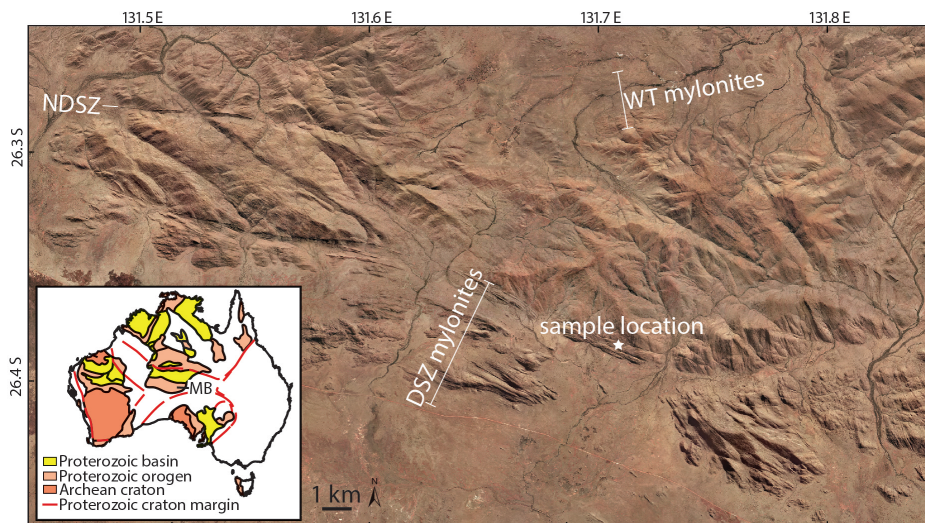
2 Geological setting

2.1 Regional geology

The Musgrave Block is located in an intraplate position close to the ~~center~~centre of the Australian continent (inset Fig. 1). Amalgamation of the different cratonic blocks took place during the Musgravian Orogeny (1120-1200 Ma), which pervasively overprinted ca. 1550 Ma gneisses (Gray, 1978; Camacho and Fanning, 1995). The Petermann Orogeny (~550 Ma) produced a series of crustal-scale fault zones, most prominently the Woodroffe Thrust and the Mann Fault (Collerson et al., 1972; Major, 1973; Bell, 1978; Camacho and Fanning, 1995; Raimondo et al., 2010; [Hawemann et al., 2018, 2019](#); Wex et al., 2017, 2018, 2019). The south-dipping Woodroffe Thrust has a top-to-the-north sense of shear, and juxtaposes the Fregon Subdomain in the south (hanging wall) against the Mulga Park Subdomain in the north (footwall). During the Musgravian Orogeny, the Mulga Park Subdomain attained amphibolite facies conditions while the Fregon Subdomain reached granulite facies (Camacho and Fanning, 1995; Scrimgeour et al., 1999; Scrimgeour and Close, 1999), and depleted the rocks of OH-bearing minerals (Wex et al., 2018; Hawemann et al., 2018).

265 The Woodroffe Thrust hosts one of the largest occurrences of pseudotachylyte worldwide
 266 (Camacho et al., 1995), but all larger scale shear zones in the hanging wall also show abundant
 267 pseudotachylyte that developed under lower crustal conditions (Camacho, 1997; Hawemann
 268 et al., 2018). Deformation in the Fregon Subdomain associated with the Petermann Orogeny
 269 is concentrated along the sub-eclogitic (~650 °C, 1.2 GPa) Davenport Shear Zone and the
 270 North Davenport Shear Zone (Fig. 1), with little discernible overprint of the earlier granulites
 271 in between (Camacho et al., 1997). The Davenport Shear Zone is a WNW-ESE-striking, strike-
 272 slip zone, with a near horizontal stretching lineation. Deformation inside the Davenport Shear
 273 Zone itself is heterogeneous and strongly localized (Hawemann et al., 2019).

274



275

Figure 1: Airborne imagery of the study area with sample location (26.3849 S, 131.7067 E) in the Davenport Shear Zone (DSZ). NDSZ = North Davenport Shear Zone, WT = Woodroffe Thrust. Image from the Department of Primary Industries and Regions, South Australia (PIRSA), 2012. Inset: Location of the Musgrave Block (MB) in between the amalgamated Australian Cratons. Modified after Evins et al. (2010)

276

2.2 Sample description

Fractured garnet is ubiquitous in the Fregon Subdomain and is not exclusively found in association with pseudotachylyte veins. However, this study focuses on a representative outcrop for which field relationships, metamorphic, and deformation conditions have been well established (F68, Hawemann et al., 2018; 26.3849 S, 131.7067 E). This outcrop consists of a quartzo-feldspathic mylonite, with millimeter-sized, granulite facies garnets, ~~that and~~ includes multiple pseudotachylyte veins and breccias. Pseudotachylytes in the studied outcrop are sheared, as indicated by elongated clasts (Fig. 2a, c), and show the same stretching lineation as the host mylonite. The original discordant relationship to the host foliation is still preserved, ~~with the crosscutting relationship most obvious in sections and cuts~~ perpendicular to the stretching lineation (Fig. 2b).

The syn-mylonitic assemblage associated ~~to with~~ the Petermann overprint of ~~the~~ felsic granulites is $Qz+Kfs+Pl+Gt+Bt+Ky+Ilm+Rt$ (mineral abbreviations following Whitney and Evans, 2010), and is similar to that of the associated sheared pseudotachylyte ($Qz+Kfs+Pl+Gt+Bt+Ky+Rt$) (Hawemann et al., 2018). The fine-grained garnet growing within the pseudotachylyte gives the rock its macroscopic caramel ~~color~~ colour in macroscopic images (Fig. 2). ~~Fractured~~ Larger fractured garnets within the granulites are clearly recognizable in polished hand specimens (Fig. 2c) and are very apparent in thin section (Fig. 3). The metamorphic conditions during shearing of this pseudotachylyte are estimated at ~600 °C and ~1.1 GPa (Fig. 7 of Hawemann et al., 2018).

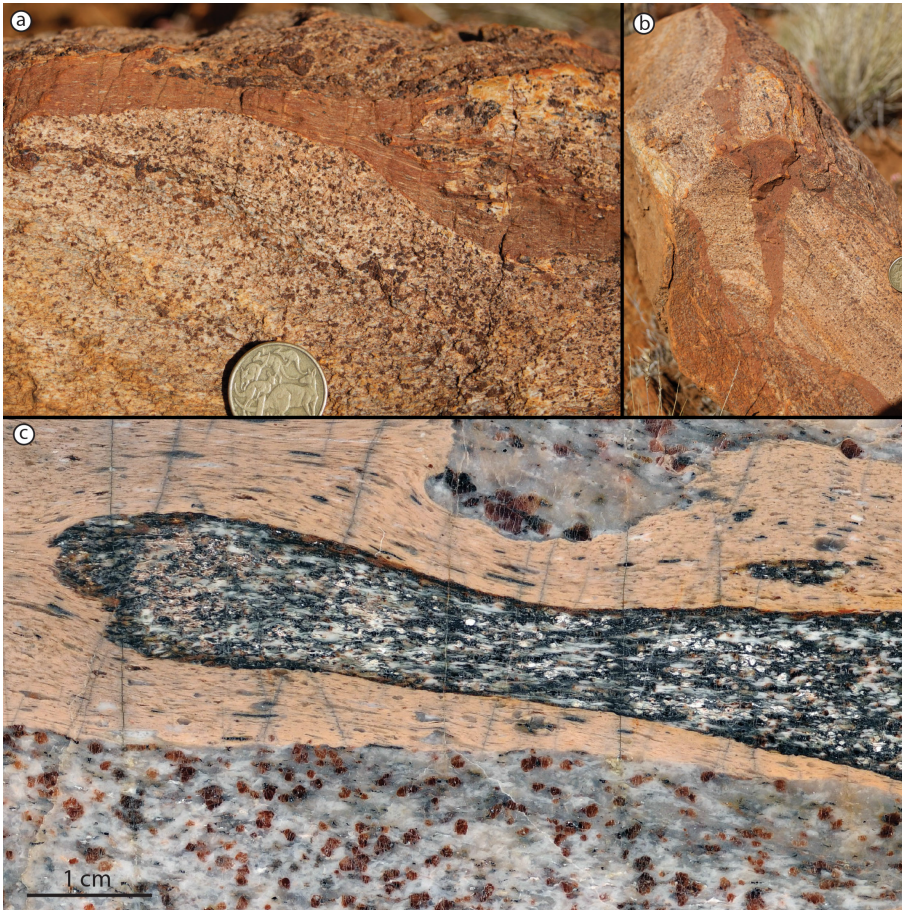


Figure 2: Sheared pseudotachylyte in a view orthogonal to the foliation of host felsic mylonite, and looking perpendicular (a) and parallel (b) to the stretching lineation. c) Polished hand specimen of a sheared pseudotachylyte breccia with the caramel-coloured foliated pseudotachylyte matrix including elongated clasts and an elongate fragment of mafic granulite. The host rock shows millimetermillimetre-sized garnets with fractures. Plane of the polished surface is perpendicular to the foliation and parallel to the stretching lineation.

3 Garnet microstructure and compositional variation

3.1 Optical microstructure

Granulite facies garnet porphyroclasts in Musgravian peraluminous gneisses mylonitized during the Petermann Orogeny are almost invariably fractured, irrespective of their proximity to pseudotachylyte (Fig. 3). Large garnet porphyroclasts (>1 mm) are typically slightly elongated with their long axis parallel to the foliation, which is attributed at least partially to resorption. Fractures in garnets often show offsets ~~in-on~~ the order of a few 100 μm . It is not possible to determine whether these offsets are primarily due to the initial shear fracture or result from subsequent sliding during ongoing ductile shear. Moreover, no consistent sense of shear can be derived from the offsets (Fig. 3a, b). These discrete fractures are sub-planar, commonly have a consistent orientation at a moderate angle to the foliation, and locally occur in conjugate sets (Fig. 3b). Wide fractures are filled with biotite, kyanite and quartz (Fig. 4b). An ~~apparent~~ later generation of unfilled ~~dilatant~~ fractures, without any discernible offset, is oriented perpendicular to both the foliation and stretching lineation (Fig. 3b). Garnet porphyroclasts commonly contain rutile exsolution lamellae and inclusions of monazite and kyanite (Fig. A1). The latter are present as aggregates with an overall prismatic shape, possibly representing pseudomorphs after sillimanite (Camacho and Fitzgerald, 2010).

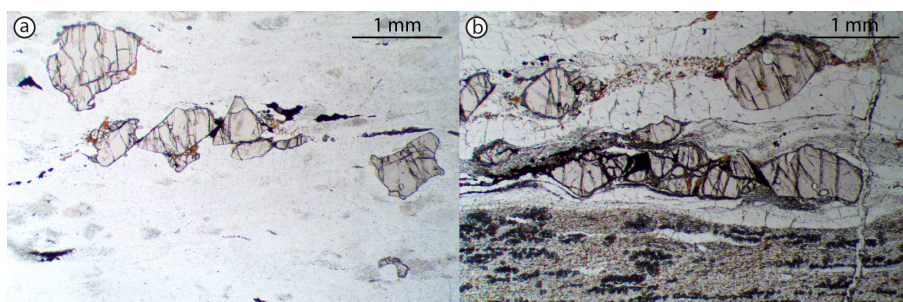


Figure 3: Thin section photomicrographs in plane polarized light of fractured garnets away from pseudotachylyte (a), and close to sheared and recrystallized pseudotachylyte in the lower part of the figure (b). The dark trails of grains elongated in the foliation of the sheared pseudotachylyte are small new garnets. Section is perpendicular to the foliation and parallel to the stretching lineation.

3.2 Analytical techniques

Quantitative mineral compositions were measured with a JEOL JXA-8200 electron probe micro-analyzer (EPMA), equipped with a tungsten filament, at the Institute of Geochemistry and Petrology at ETH Zurich (Switzerland). Natural standards were used for quantification, and, when available, natural garnet standards were preferred. To reach a spatial resolution of about 1 μm , an acceleration voltage of 10 kV was set (Fig. 8 in Hofer and Brey, 2007). Elemental maps were acquired using energy wavelength-dispersive spectrometers in parallel for calcium, to increase the signal-to-noise ratio. Backscatter electron images (BSE), energy-dispersive spectrometry (EDS) and electron backscatter diffraction (EBSD) mapping was carried out on a Quanta 200F field emission gun (FEG) scanning electron microscope at the ScopeM (Scientific Center for Optical and Electron Microscopy, ETH Zurich). EBSD maps were collected with an acceleration voltage of 20 kV, a sample tilt of 70° and a working distance of 15 mm. Data were post-processed using chemical indexing with the software OIM 7 by EDAX. When necessary, three different clean-up techniques were used: ~~neighbor~~neighbor confidence index correlation, ~~neighbor~~neighbor orientation correlation and grain dilation. Point and map analyses, as well as BSE images, were combined for correlation with optical microscope images in a QGIS-project (Open Source Geospatial foundation). Two lamellae were cut with a focused ion beam (FIB) for transmission electron microscopy (TEM). The

340 microscope used for TEM is a Tecnai F30 with a FEG source operated at 300 kV and equipped
341 with a Gatan 794 MultiScan CCD (ScopeM, ETH Zurich).

342 3.3 ~~Compositional~~Compositional gradients

343 Granulite facies garnet has a homogeneous composition of X_{Alm} 0.54, X_{Pyp} 0.40, X_{Grs} 0.03, X_{Sps}
344 0.03, whereas garnet neocrystallized during the Petermann Orogeny is more Ca-rich (X_{Alm}
345 0.48, X_{Pyp} 0.28, X_{Grs} 0.22, X_{Sps} 0.02). Grain boundaries of granulite facies garnet and fractures

346 are decorated with a Ca-enriched rim, 20 to 40 μm wide (Fig. 4c). ~~The enrichment is mostly~~
347 ~~concentric, also affects resorbed areas of the garnet and is therefore most likely the result of~~
348 ~~diffusion (Camacho et al., 2009). The length-scale for variation in Fe (X_{Alm}) and Mg (X_{Pyp}) is~~
349 ~~identical to that for Ca (X_{Grs}), whereas the Mn content (X_{Sps}) does not show any variation (Fig~~
350 ~~4d). The diffusion length for iron and magnesium is identical to Ca, while the manganese~~
351 ~~content does not show any variations (Fig 4c).~~ Neocrystallized garnet is present where the

352 grain boundary is in contact with, or close to, plagioclase. The outermost rim of remnant
353 garnet has the same composition as the neocrystallized garnet (Fig. 4d, profile 1). The
354 granulitic-granulite-facies plagioclase is partially transformed to a more Na-rich plagioclase
355 with needle shaped inclusions of kyanite (bottom of Fig. 4e). This reaction provides Ca for the
356 observed diffusion into garnet (Camacho et al., 2009).

357 Along fractures across the porphyroclasts, the Ca enrichment is narrower than along the grain
358 boundaries and the grossular component only reaches up to about X_{Grs} 0.1 (Fig. 4d, profile 2).
359 Compositional gradients are also present around inclusions in garnet connected to the outer
360 garnet boundary, providing evidence of Ca diffusion along grain boundaries (right part of Fig.
361 4c, profile 3 in Fig 4d). Profile 4 (Fig. 4d) was measured next to a kyanite inclusion: the
362 diffusion length is still comparable to those of profiles 1-3, but Ca concentrations are much

Commented [n1]: This text is eliminated here because it is interpretation and best considered the discussion section below.

363 lower. Ca probably diffused along fractures (invisible in the plane of the thin section) towards
364 the inclusion. In summary, the diffusion length at the original grain boundaries is maximized
365 where in contact with plagioclase, and otherwise constant at about 20 μm width. However,
366 variations in diffusion lengths do occur around garnet fragments, without any correlation with
367 the proximity to plagioclase, although the exact relationship in the third dimension is
368 unknown. Surfaces with limited diffusion can often be identified as fracture surfaces, which
369 were exposed to diffusion for a shorter time than original grain boundaries (Fig. 4e). Fractures
370 oriented perpendicular to the foliation and stretching lineation lack any signs of diffusion and
371 are therefore interpreted as later stage ~~dilatant~~ extensional fractures.

372 Some garnets display more complicated compositional patterns, with zones $>100\ \mu\text{m}$ of Ca
373 enrichment extending into the porphyroclast's interior, which are not associated with
374 fractures (e.g. the garnet fragment on the far right in Figure 4e). EBSD-analysis highlights that
375 the three fragments in the right part of Figure 4e most likely originated from the same grain,
376 as they share a common rotation axis (Fig. 4f). The ~~colors~~ colours in the inverse pole figure
377 map are not solid, reflecting slight variations of orientation within the crystal. Furthermore,
378 the image quality map shows areas of suppressed Kikuchi patterns (grey value) suggestive of
379 higher dislocation density and therefore possible subgrain boundaries (Fig. 4f). The
380 misorientation angle map (Fig. 4g) reveals a complex pattern of varying crystal orientation (all
381 within the order of 5°) in the fragments, with very distributed zones connected to the edges
382 of the crystal, triangular-shaped zones of misorientation (upper left of Fig. 4g), and discrete
383 zones (lower right of Fig. 4g). The discrete zones of misorientation, about $5\ \mu\text{m}$ wide, correlate
384 well with the Ca-enriched zones (compare Fig. 4e, f, garnet fragment on the right).

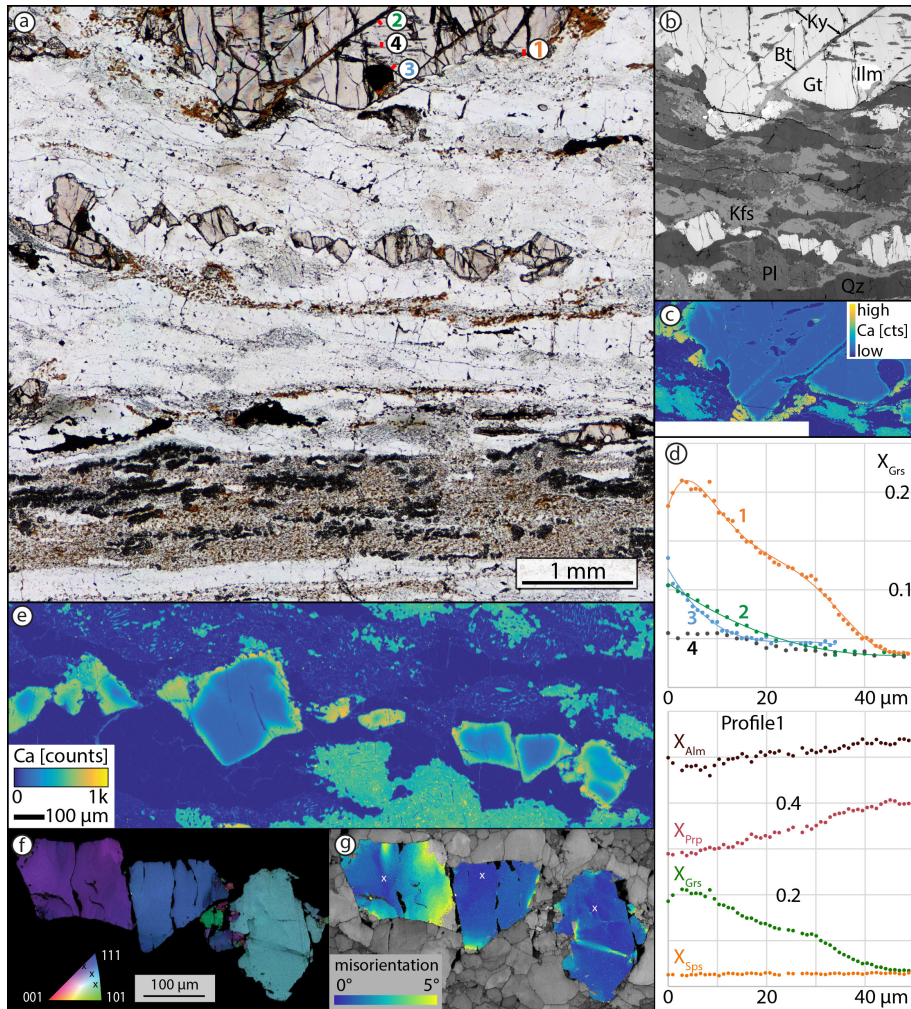


Figure 4: a) Plane polarized light image of thin section with fractured garnets and a pseudotachylyte vein in the lower part of the image. b) BSE image of the upper area of (a), with same scale as (a). c) EPMA X-ray map for Ca reveals an enrichment the-in thin diffusion gradational rims along grain boundaries, and fractures, and within neocrystallized garnet (euhedral, orange). d) Grossular component profiles indicated on (a) (Profile-profile lines are not to scale for the sake of visibility); and compositional profiles for four garnet end-members in profile 1. e) EPMA X-ray map for Ca for the garnet fragments in the center of (a). Note the uneven colours in the plagioclase and the blue kyanite needles. f) Inverse pole figure map with superimposed image quality map for garnet fragments shows a common rotation pole. g) Misorientation map relative to reference point for each fragment reveals internal lattice distortions.

3.4 Texture of deformed garnets

Two to three orientations of fractures are generally present in a single garnet crystal and coincide with the trace of the (101)-plane derived from EBSD data (Fig. 5a, b). Fracture set (I) in the example of Figure 5a is often associated with a relative rotation of both sides, as visible from the difference in ~~color~~colour. In the lower part of the grain, where the fracture density is very high, more subgrains are present. The subgrain spatial density increases towards the original grain boundary and some subgrains are “eroded” by ductile shearing and strung out along the foliation. This demonstrates that ductile shearing outlasted subgrain formation and fracturing. ~~Subgrains of less than 10 µm in size formed in the fracture plane (III in Fig. 5a).~~ The fractures described above are all crosscut by ~~dilatant~~ extensional fractures (set ~~I~~II in Fig. 5a), oriented perpendicular to the stretching lineation and foliation, which do not show any associated distortion of the crystal lattice.

The garnet porphyroclast of Figure 5c shows a central fracture as well as a set of two other parallel fractures. The central fracture is the only one with significant offset and is filled with kyanite and quartz. This fracture displays misorientations of more than 5° towards the right-hand side of the scan, but none towards the left-hand side. In the lower left corner of the fragment, subgrains are observed with misorientations, relative to the average orientation, typically in the range of 10°. Misorientation axes are often parallel to (111) and (101). The lowermost fragment shows a wide zone of progressive rotation. The chemical profile in Figure 5e shows the highest Ca counts towards the boundaries of the porphyroclasts and, internally, towards two fractures. The larger fracture with apparent offset of the two garnet fragments exhibits a less well-developed zone of calcium~~Ca enrichment~~~~efficient calcium diffusion~~ when compared to the tight fracture with introduced lattice distortion.

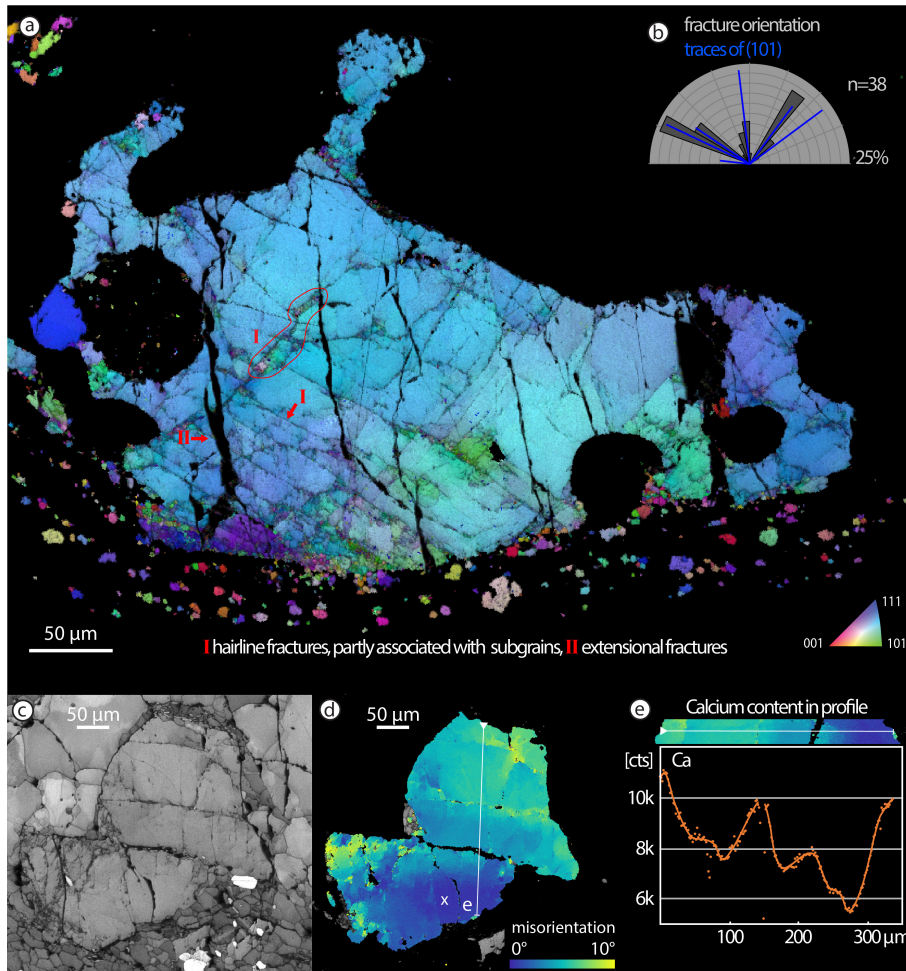


Figure 5: a) Inverse pole figure map of fractured garnet with three dominant orientations of fractures. b) Rose diagram correlating traced fracture orientations and (101)-planes for garnet in (a). c) Image quality map of a fragmented garnet with subgrains. d) Misorientation plot (with respect to the point marked with the white x) shows long wavelength bending in the lower fragment and distortion in the crystal lattice induced by a fracture in the upper fragment. e) EDS-calcium counts for the profile marked as a thin white line in (d).

3.5 TEM investigations

The garnet fragment of Figure 4g was further investigated using TEM, as it includes a narrow zone of misorientation without fractures and is therefore suitable for preparation of FIB-lamellae. As visible in Figure 6a (around profile 1), the image quality map shows a well-defined narrow, darker [grey](#) band, possibly indicating high dislocation density. The zone is even more evident in the misorientation plot (Fig. 6b) and changes from about 5 μm wide, with discrete boundaries to the right, to a wider ($> 10 \mu\text{m}$) band towards the left of the image. In the upper left part of the image, a subgrain boundary with $> 5^\circ$ misorientation transitions into a zone of gradual misorientation. The misorientation axis is consistently parallel to (101) with minor rotation around (111) (Fig. 6c, Fig. A2). Misorientation profiles reveal a slight asymmetry within the narrow band, where the lower boundary appears to be sharper. Misorientation changes more gradually within the wider portion of the misorientation band. Locally, subgrains developed with discrete boundaries, documenting a misorientation of usually around $5\text{-}10^\circ$ (profile 3 in Fig. 6d). The FIB-lamella was cut across the narrow band of misorientations (Fig. 6e). The lower boundary corresponds to a narrow discrete zone, without visible dislocations (Fig. 6f). The upper boundary is marked by a series of dislocation walls and only a few free dislocations are visible, which are often organized in arrays (Fig. 6g, h). The existence of dislocation walls [and subgrain boundaries](#) indicates recovery by dislocation climb [\(e.g., Hobbs, 1968; Passchier and Trouw, 2005\)](#).

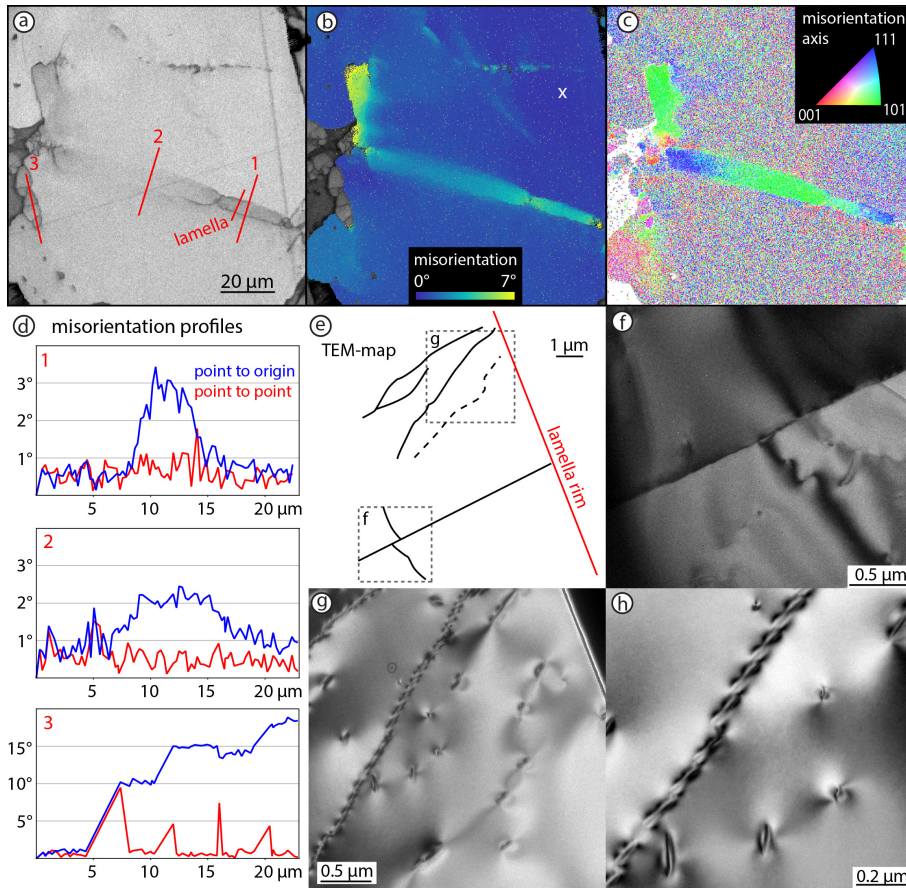


Figure 6: a) Image quality map of the garnet fragment (compare Fig. 4f) with darker zones that can be interpreted as areas of high dislocation density and location of the FIB-lamella. b) Misorientation plot with respect to the reference point (marked with the white x) shows a discrete zone of misorientation, which has discrete boundaries in the right part of the image, but is more distributed towards the left. c) Misorientation axis plot with respect to the average orientation of the grain shows a consistent rotation around the (101) and (111) axes. For pole figure plots, see Fig. A2. d) Misorientation profiles indicated in a), for (1) the narrow zone, (2) the more distributed zone and (3) for subgrains. e) Overview sketch of the FIB-lamella used for TEM-analysis for correlation with the EBSD data. f) Sharp contrast boundary in the lower part of the lamella. g) Two dislocation walls with a few free dislocations, which are partly linking up parallel to the dislocation walls. h) Detail of the center-centre of (g)

435 4 Discussion

436 Garnets in this study show evidence for both brittle and ductile deformation under relatively
437 low temperatures of about 600 °C, as inferred from synchronous diffusion and ductile
438 shearing of pseudotachylyte (Hawemann et al, 2018). This is ~~well~~ below the experimentally
439 determined values for the onset of crystal-plastic deformation of garnet ([Wang and Ji, 1999](#))
440 ~~at the higher strain rates considered typical of mylonitic shear zones ($> 10^{-14} \text{ s}^{-1}$) ($> 850 \text{ °C}$;~~
441 ~~Wang and Ji, 1999).~~ In contrast to experiments, many natural examples (Vollbrecht et al.,
442 2006; Bestmann et al., 2008; Austrheim et al., 2017) indicate crystal plasticity of garnet at
443 lower temperatures between 650 °C and 700 °C, ~~challenging the reliability of extrapolation of~~
444 ~~experimental data to natural conditions.~~

445 The presence of microstructures and -textures consistent with dislocation climb and recovery,
446 as well as subgrain rotation, in garnet at around 600 °C is in agreement with previous studies
447 (Bestmann et al., 2008; Massey et al., 2011). No evidence for grain boundary sliding is
448 observed, since subgrains show rotation around a specific crystallographic axis. Rotation
449 around (111) and (101) is in accordance with the slip systems described by Voegelé et al.
450 (1998).

451 Multiple generations of overprinting fractures with different orientation demonstrate
452 repeated fracturing events. ~~Tensile-Extensional~~ fractures do not show any induced lattice
453 distortion or diffusion and therefore occurred after the temperature ~~was had decreased to~~
454 ~~values~~ too low for diffusion (Camacho et al., 2009), possibly during exhumation (compare
455 Prior, 1993 and Ji et al., 1997).

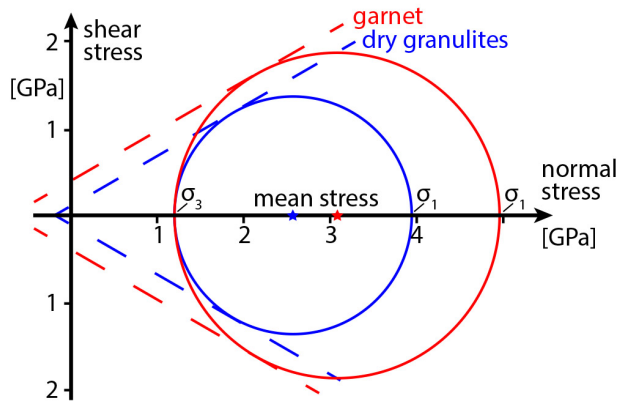
456 In contrast to the observations of Austrheim et al. (2017), ~~and~~ Papa et al. (2018) ~~and~~ Petley-
457 ~~Ragan et al. (2019)~~ from other examples in the deep continental crust, no “explosive

458 fracturing" ~~or~~ "shattering" or "fragmentation" of garnet is observed in relict porphyroclasts
 459 immediately adjacent to pseudotachylyte. The fractures described here are generally planar
 460 and often consistently oriented, in some cases showing single and conjugate shear offsets.
 461 Fractured garnet is not restricted to the boundary with pseudotachylyte and is still present
 462 even in samples without pseudotachylyte, where the nearest pseudotachylyte is possibly
 463 many ~~meters~~ metres or more away. Fracturing in this case cannot be related to thermal shock
 464 (Papa et al., 2018) or localized high stress due to (seismic) fracture propagation (Austrheim et
 465 al., 2017; Petley-Ragan et al., 2019), but must reflect a larger scale distribution of differential
 466 stresses in the lower crust that were, at least transiently, high enough to cause brittle garnet
 467 failure (Hawemann et al., 2019). This could be due to stress pulses from earthquakes in the
 468 shallower brittle regime (Trepmann and Stöckhert, 2002; Ellis and Stöckhert, 2004; Jamtveit
 469 et al., 2018a, b; Jamtveit et al., in press) or a more local, lower crustal source due to jostling
 470 of less-deformed strong blocks within an irregular shear zone network (Hawemann et al.,
 471 2019).
 472 The narrower Ca diffusion profiles on some fractures relative to garnet rims and crosscutting
 473 relationships suggest that fracturing was recurrent under sub-eclogite facies metamorphic
 474 conditions, as also indicated by the occasional presence of kyanite in ~~some of~~ some fractures.
 475 The presence of kyanite needles and the absence of zoisite/clinozoisite or epidote, as a
 476 breakdown product of plagioclase during sub-eclogitic metamorphism (Fig. 3b), indicate
 477 relatively dry lower crustal conditions (Hawemann et al., 2018). According to Wayte et al.
 478 (1989), this indicates a water activity of < 0.004, calculated for rocks of comparable
 479 composition and P-T conditions. However, new biotite did form in ~~dilatant~~ fractures across
 480 relict garnet, so conditions were probably not strictly anhydrous. The sheared and
 481 recrystallized pseudotachylyte developed a similar synkinematic assemblage as the host

482 mylonite, demonstrating that there is also no marked partitioning of water into the frictional
483 melt, which implies little free or bound water available in the original source rock (e.g. Wex
484 et al., 2018). The effect of pore-fluid pressure on the effective confining pressure must
485 therefore have been negligible.

486 As reported in Hawemann et al. (2019), the dynamically recrystallized quartz grain size and
487 microstructure in the host rock mylonites indicates that long-term flow stresses were not
488 particularly high, on the order of less than 10 MPa. The ambient pressure of ca. 1.1-1.2 GPa
489 determined for the host rocks should therefore be close to the lithostatic value (Mancktelow,
490 2008). Figure 7 shows a simple linear plot of the Mohr-Coulomb failure criterion for an angle
491 of internal friction of 30° (coefficient $\mu = 0.6$), a lithostatic load of 1.2 GPa, and no pore fluid
492 pressure. This plot is only qualitative, since the angle of internal friction could decrease
493 towards higher pressure ([Shimada et al., 1983](#)). However, the summary of experimental
494 results in Byerlee (1978) indicates that there may be little change at least up to pressures
495 similar to those considered here. It follows that the differential stress for fracture initiation
496 must have been of the same order as the confining pressure (Fig. 7). As discussed in detail in
497 Hawemann et al. (2019), such high differential stresses, leading to garnet fracture and the
498 development of abundant pseudotachylyte, can only have been transient and presumably
499 related to repeated short-term seismic events in the lower continental crust ([Hawemann et](#)
500 [al., 2018](#); [Jamtveit et al, 2018a, b](#); [Menegon et al., 2017](#)). The lack of shattered garnet adjacent
501 to pseudotachylyte in these samples may reflect drier conditions relative to those in the
502 Bergen Arc (Austrheim et al., 2017) and Mont Mary (Papa et al., 2018). The samples studied
503 could therefore represent one end-member of the lower continental crust, where
504 deformation occurs without the initial presence or influx of free water during fracturing and
505 subsequent crystal-plastic deformation.

506



507

Figure 7: Mohr circles for fracturing of dry granulites and garnet at 1.2 GPa lithostatic load

508

509 5 Conclusions

510 In dry lower continental crust deformed under conditions of ca. 600 °C and 1.1 GPa, garnet
 511 shows both single and conjugate sets of shear fractures, fractures with associated subgrains
 512 and induced lattice damage around fractures, subgrain formation without fracturing, and
 513 late-stage ~~dilatant~~ extensional fractures. Most of these fractures show a strong
 514 crystallographic control, with fracturing preferentially occurring along the (101) planes of
 515 garnet. Dynamic recrystallization is evident from inferred subgrain rotation recrystallization
 516 and recovery is manifested by the presence of dislocation walls. The observed
 517 microstructures of garnets are interpreted to record transient high stresses during deep
 518 seismic events in the lower crustal Fregon Subdomain. ~~This which~~ is also indicated by the
 519 abundant occurrence of pseudotachylyte developed under similar lower crustal conditions
 520 and, possibly, by the variability of recrystallized quartz grain sizes including values down to a
 521 few ~~micrometers~~ micrometres (Hawemann et al. 2009b). The studied example represents one

end-member of lower continental crustal ~~behavior~~behaviour where, because of earlier metamorphic dehydration and the intracratonic position well removed from the plate margin, rocks were initially dry and water was not introduced during fracturing and crystal-plastic deformation.

Author contributions

All authors listed took part in at least two of the three field seasons. NM assisted FH in the data collection and interpretation. AC's and GP's knowledge in the field of garnet deformation and diffusion processes were crucial in preparing the manuscript. SW contributed to the microprobe and SEM work. FH prepared the manuscript with contributions from all co-authors.

Competing interests

The authors declare that they have no conflict of interest.

Acknowledgements

We want to thank Matthias Konrad-Schmolke and an anonymous reviewer for their critical comments which improved the manuscript. We gratefully acknowledge permission granted to work on the Anangu Pitjantjatjara Yankunytjatjara Lands (APY) to carry out our field work in the area. The Northern Territory Geological Survey (NTGS) and Basil Tikoff (Department of Geoscience, University of Wisconsin) are thanked for their logistical support and the Nicolle family of Mulga Park station for their hospitality. The Scientific Center for Optical and Electron Microscopy (ScopeM) provided the facilities for the scanning electron microscopy work, and help by Karsten Kunze, Luiz Morales and Fabian Gramm is especially acknowledged. Luca Menegon is thanked for his review of the first author's doctoral thesis. This project was financed by the Swiss National Science Foundation (SNF) grant 200021_146745 and by the

545 University of Padova (BIRD175145/17: The geological record of deep earthquakes: the
546 association pseudotachylyte-mylonite).

547

548 **Data ~~Availability~~Availability**

549 All data used in this paper can be accessed through the depository of the Open Science
550 Framework here: <https://osf.io/yrzgh/>

551

552 **References**

553 Austrheim, H., Erambert, M. and Boundy, T. M.: Garnets recording deep crustal earthquakes, Earth
554 and Planetary Science Letters, 139(1–2), 223–238, doi:10.1016/0012-821X(95)00232-2, 1996.

555 Austrheim, H., Dunkel, K. G., Plümpner, O., Ildefonse, B., Liu, Y. and Jamtveit, B.: Fragmentation of
556 wall rock garnets during deep crustal earthquakes, Science Advances, 3(2), e1602067,
557 doi:10.1126/sciadv.1602067, 2017.

558 [Angiboust, S., Yamato, P., Hertgen, S., Hyppolito, T., Bebout, G.E., Morales, L.: Fluid pathways and
559 high-P metasomatism in a subducted continental slice \(Mt. Emilius klippe, W. Alps\), Journal of
560 Metamorphic Geology, 35, 471–492, 2017.](#)

561 Baxter, E. F. and Scherer, E. E.: Garnet Geochronology: Timekeeper of Tectonometamorphic
562 Processes, Elements, 9(6), 433–438, doi:10.2113/gselements.9.6.433, 2013.

563 [Behr, W.M., Platt, J.P., 2011: A naturally constrained stress profile through the middle crust in an
564 extensional terrane. Earth and Planetary Science Letters 303, 181-192, 2011.](#)

565 Bell, T. H.: Progressive deformation and reorientation of fold axes in a ductile mylonite zone: the
566 Woodroffe thrust, Tectonophysics, 44(1), 285–320, 1978.

567 Bestmann, M., Habler, G., Heidelbach, F. and Thöni, M.: Dynamic recrystallization of garnet and
568 related diffusion processes, Journal of Structural Geology, 30(6), 777–790,
569 doi:10.1016/j.jsg.2008.02.007, 2008.

570 Caddick, M. J., Konopasek, J. and Thompson, A. B.: Preservation of Garnet Growth Zoning and the
571 Duration of Prograde Metamorphism, Journal of Petrology, 51(11), 2327–2347,
572 doi:10.1093/petrology/egq059, 2010.

573 Camacho, A. and Fanning, C. M.: Some isotopic constraints on the evolution of the granulite and
574 upper amphibolite facies terranes in the eastern Musgrave Block, central Australia, Precambrian
575 Research, 71(1), 155–181, 1995.

576 Camacho, A. and Fitz Gerald, J. D.: Misidentification of oxide phases and of twinned kyanite:
577 implications for inferred P-T histories of the Musgrave Block, central Australia, *Journal of the Virtual*
578 *Explorer*, 35, doi:10.3809/jvirtex.2011.00275, 2010.

579 Camacho, A., Vernon, R. H. and Fitz Gerald, J. D.: Large volumes of anhydrous pseudotachylyte in the
580 Woodroffe Thrust, eastern Musgrave Ranges, Australia, *Journal of Structural Geology*, 17(3), 371–
581 383, 1995.

582 Camacho, A., Compston, W., McCulloch, M. and McDougall, I.: Timing and exhumation of eclogite
583 facies shear zones, Musgrave Block, central Australia, *J. metamorphic Geol.*, 15, 735–751, 1997.

584 Camacho, A., Yang, P. and Frederiksen, A.: Constraints from diffusion profiles on the duration of
585 high-strain deformation in thickened crust, *Geology*, 37(8), 755–758, 2009.

586 Collerson, K. D., Oliver, R. L. and Rutland, R. W. R.: An example of structural and metamorphic
587 relationships in the Musgrave orogenic belt, central Australia, *Journal of the Geological Society of*
588 *Australia*, 18(4), 379–393, doi:10.1080/00167617208728776, 1972.

589 Dalziel, I. W. D. and Bailey, S. W.: Deformed garnets in a mylonitic rock from the Grenville Front and
590 their tectonic significance, *American Journal of Science*, 266(7), 542–562, doi:10.2475/ajs.266.7.542,
591 1968.

592 [Ellis, S., Stöckhert, B.: Elevated stresses and creep rates beneath the brittle-ductile transition caused](#)
593 [by seismic faulting in the upper crust. *Journal of Geophysical Research*, 109, B05407, 2017.](#)

594 [Engi, M., Giuntoli, F., Lanari, P., Burn, M., Kunz, B. E., and Bouvier, A.-S.: Pervasive eclogitization due](#)
595 [to brittle deformation and rehydration of subducted basement: Effects on continental recycling?.](#)
596 [Geochemistry Geophysics Geosystems, 19, https://doi.org/10.1002/2017GC007215, 2018.](#)

597 Evins, P. M., Smithies, R. H., Howard, H. M., Kirkland, C. L., Wingate, M. T. D. and Bodorkos, S.:
598 Redefining the Giles Event within the setting of the 1120-1020 Ma Ngaanyatjarra Rift, West
599 Musgrave Province, Central Australia, *Geological Society of Western Australia*, East Perth, W.A.,
600 2010.

601 Gray, C. M.: Geochronology of granulite - facies gneisses in the western Musgrave Block, Central
602 Australia, *Journal of the Geological Society of Australia*, 25(7–8), 403–414,
603 doi:10.1080/00167617808729050, 1978.

604 [Giuntoli, F., Lanari, P., and Engi, M.: Deeply subducted continental fragments – Part 1: Fracturing,](#)
605 [dissolution–precipitation, and diffusion processes recorded by garnet textures of the central Sesia](#)
606 [Zone \(western Italian Alps\), *Solid Earth*, 9, 167–189, https://doi.org/10.5194/se-9-167-2018, 2018.](#)

607 Hawemann, F., Mancktelow, N. S., Wex, S., Camacho, A. and Pennacchioni, G.: Pseudotachylyte as
608 field evidence for lower-crustal earthquakes during the intracontinental Petermann Orogeny
609 (Musgrave Block, Central Australia), *Solid Earth*, 9(3), 629–648, doi:10.5194/se-9-629-2018, 2018.

610 Hawemann, F., Mancktelow, N. S., Pennacchioni, G., Wex, S. and Camacho, A.: Weak and slow,
611 strong and fast: How shear zones evolve in a dry continental crust (Musgrave Ranges, Central
612 Australia), *Journal of Geophysical Research: Solid Earth*, doi:10.1029/2018JB016559, 2019.

613 [Hobbs, B.E.: Recrystallisation of single crystals of quartz. *Tectonophysics*, 6, 353-401, 1968.](#)

Hofer, H. E. and Brey, G. P.: The iron oxidation state of garnet by electron microprobe: Its determination with the flank method combined with major-element analysis, *American Mineralogist*, 92(5–6), 873–885, doi:10.2138/am.2007.2390, 2007.

[Jamtveit, B., Ben-Zion, Y., Renard, F., Austrheim, H., 2018: Earthquake-induced transformation of the lower crust. *Nature* 556, 487–491, 2018a.](#)

[Jamtveit, B., Moulas, E., Andersen, T.B., Austrheim, H., Corfu, F., Petley-Ragan, A., Schmalholz, S.M.: High pressure metamorphism caused by fluid induced weakening of deep continental crust. *Scientific Reports*, 8, 17011, 2018b.](#)

[Jamtveit, B., Petley-Ragan, A., Incel, S., Dunkel, K.G., Aupart, C., Austrheim, H., Corfu, F., Menegon, L., Renard, F.: The effects of earthquakes and fluids on the metamorphism of the lower continental crust, *Journal of Geophysical Research: Solid Earth*, doi:10.1029/2018jb016461, in press.](#)

Ji, S., Zhao, P. and Saruwatari, K.: Fracturing of garnet crystals in anisotropic metamorphic rocks during uplift, *Journal of Structural Geology*, 19(5), 603–620, 1997.

Karato, S., Wang, Z., Liu, B. and Fujino, K.: Plastic deformation of garnets: systematics and implications for the rheology of the mantle transition zone, *Earth and Planetary Science Letters*, 130(1–4), 13–30, 1995.

Kirkpatrick, J. D. and Rowe, C. D.: Disappearing ink: How pseudotachylytes are lost from the rock record, *Journal of Structural Geology*, 52, 183–198, doi:10.1016/j.jsg.2013.03.003, 2013.

[Konrad-Schmolke, M., O'Brien, P. J., Heidelbach, F.: Compositional reequilibration of garnet: the importance of sub-grain boundaries. *European Journal of Mineralogy* 19, 431–438, 2007.](#)

Kunze, K., Wright, S. I., Adams, B. L. and Dingley, D. J.: Advances in automatic EBSD single orientation measurements, *Texture, Stress, and Microstructure*, 20(1–4), 41–54, 1993.

Lasaga, A. C.: Geospeedometry: an extension of geothermometry, in *Kinetics and equilibrium in mineral reactions*, pp. 81–114, Springer. [online] Available from: http://link.springer.com/chapter/10.1007/978-1-4612-5587-1_3 (Accessed 28 May 2017), 1983.

Major, R. B.: Explanatory Notes for the Woodroffe 1: 250 000 Geological Map SG/52-12 (1st ed.). Adelaide, Australia: Geological Survey of South Australia, 1973.

Massey, M. A., Prior, D. J. and Moecher, D. P.: Microstructure and crystallographic preferred orientation of polycrystalline microgarnet aggregates developed during progressive creep, recovery, and grain boundary sliding, *Journal of Structural Geology*, 33(4), 713–730, doi:10.1016/j.jsg.2010.12.009, 2011.

[Menegon, L., Pennacchioni, G., Malaspina, N., Harris, K., & Wood, E., 2017: Earthquakes as precursors of ductile shear zones in the dry and strong lower crust. *Geochemistry, Geophysics, Geosystems*, 18. <https://doi.org/10.1002/2017GC007189>, 2017.](#)

Papa, S., Pennacchioni, G., Angel, R. J. and Faccenda, M.: The fate of garnet during (deep-seated) coseismic frictional heating: The role of thermal shock, *Geology*, 46(5), 471–474, doi:10.1130/G40077.1, 2018.

[Passchier, C.W., Trouw, R.A.J.: *Microtectonics* \(2nd Edition\), Springer, Heidelberg, 366 pp., 2005.](#)

653 [Petley-Ragan, A., Dunkel, K. G., Austrheim, H., Ildefonse, B., Jamtveit, B.: Microstructural records of](#)
 654 [earthquakes in the lower crust and associated fluid-driven metamorphism in plagioclase-rich](#)
 655 [granulites. Journal of Geophysical Research: Solid Earth, 123, 3729–3746.](#)
 656 <https://doi.org/10.1029/2017JB015348>, 2018

657 [Petley-Ragan, A., Ben-Zion, Y., Austrheim, H., Ildefonse, B., Renard, F., Jamtveit, B.: Dynamic](#)
 658 [earthquake rupture in the lower crust. Science Advances, 5, doi: 10.1126/sciadv.aaw0913, 2019.](#)

659 Prior, D. J.: Sub-critical fracture and associated retrogression of garnet during mylonitic deformation,
 660 Contributions to Mineralogy and Petrology, 113(4), 545–556, doi:10.1007/BF00698322, 1993.

661 Prior, D. J., Wheeler, J., Brenker, F. E., Harte, B. and Matthews, M.: Crystal plasticity of natural
 662 garnet: New microstructural evidence, Geology, 28(11), 1003, doi:10.1130/0091-
 663 7613(2000)28<1003:CPONGN>2.0.CO;2, 2000.

664 Prior, D. J., Wheeler, J., Peruzzo, L., Spiess, R. and Storey, C.: Some garnet microstructures: an
 665 illustration of the potential of orientation maps and misorientation analysis in microstructural
 666 studies, Journal of Structural Geology, 24(6–7), 999–1011, doi:10.1016/S0191-8141(01)00087-6,
 667 2002.

668 Raimondo, T., Collins, A. S., Hand, M., Walker-Hallam, A., Smithies, R. H., Evins, P. M. and Howard, H.
 669 M.: The anatomy of a deep intracontinental orogen, Tectonics, 29(4), n/a-n/a,
 670 doi:10.1029/2009TC002504, 2010.

671 [Shimada, M., Cho, A., Yukutake, H., ~~1983~~: Fracture strength of dry silicate rocks at](#)
 672 [high confining pressures and activity of acoustic emission. Tectonophysics 96, 159–](#)
 673 [172. doi:10.1016/0040-1951\(83\)90248-2, 1983.](#)

674

675 Sibson, R. H.: Generation of pseudotachylite by ancient seismic faulting, Geophysical Journal
 676 International, 43(3), 775–794, 1975.

677 Sibson, R. H. and Toy, V. G.: The habitat of fault-generated pseudotachylite: Presence vs. absence of
 678 friction-melt, in Geophysical Monograph Series, vol. 170, edited by R. Abercrombie, A. McGarr, H.
 679 Kanamori, and G. Di Toro, pp. 153–166, American Geophysical Union, Washington, D. C. [online]
 680 Available from: <http://www.agu.org/books/gm/v170/170GM16/170GM16.shtml> (Accessed 21
 681 January 2014), 2006.

682 Toy, V. G., Ritchie, S. and Sibson, R. H.: Diverse habitats of pseudotachylites in the Alpine Fault Zone
 683 and relationships to current seismicity, Geological Society, London, Special Publications, 359(1), 115–
 684 133, doi:10.1144/SP359.7, 2011.

685 Trepmann, C. A. and Stöckhert, B.: Cataclastic deformation of garnet: a record of synseismic loading
 686 and postseismic creep, Journal of Structural Geology, 24(11), 1845–1856, doi:10.1016/S0191-
 687 8141(02)00004-4, 2002.

688 Voegelé, V., Cordier, P., Sautter, V., Sharp, T. G., Lardeaux, J. M. and Marques, F. O.: Plastic
 689 deformation of silicate garnets, Physics of the Earth and Planetary Interiors, 108(4), 319–338,
 690 doi:10.1016/S0031-9201(98)00111-3, 1998.

691 Vollbrecht, A., Pawlowski, J., Leiss, B., Heinrichs, T., Seidel, M. and Kronz, A.: Ductile deformation of
 692 garnet in mylonitic gneisses from the Münchberg Massif (Germany), Tectonophysics, 427(1–4), 153–
 693 170, doi:10.1016/j.tecto.2006.05.024, 2006.

694 Wang, Z. and Ji, S.: Deformation of silicate garnets; brittle-ductile transition and its geological
695 implications, *The Canadian Mineralogist*, 37(2), 525, 1999.

696 Wayte, G. J., Worden, R. H., Rubie, D. C. and Droop, G. T. R.: A TEM study of disequilibrium
697 plagioclase breakdown at high pressure: the role of infiltrating fluid, *Contributions to Mineralogy
698 and Petrology*, 101(4), 426–437, doi:10.1007/BF00372216, 1989.

699 Wex, S., Mancktelow, N. S., Hawemann, F., Camacho, A. and Pennacchioni, G.: Geometry of a large-
700 scale, low-angle, mid-crustal thrust (Woodroffe Thrust, central Australia): Geometry of a mid-crustal
701 thrust, *Tectonics*, doi:10.1002/2017TC004681, 2017.

702 Wex, S., Mancktelow, N. S., Hawemann, F., Camacho, A. and Pennacchioni, G.: Inverted distribution
703 of ductile deformation in the relatively “dry” middle crust across the Woodroffe Thrust, central
704 Australia, *Solid Earth*, 9(4), 859–878, doi:10.5194/se-9-859-2018, 2018.

705 Wex, S., Mancktelow, N. S., Camacho, A. and Pennacchioni, G.: Interplay between seismic fracture
706 and aseismic creep in the Woodroffe Thrust, central Australia – Inferences for the rheology of
707 relatively dry continental mid-crustal levels, *Tectonophysics*, 758, 55–72,
708 doi:10.1016/j.tecto.2018.10.024, 2019.

709

710

711

712

713

714

715

716 **Appendix**

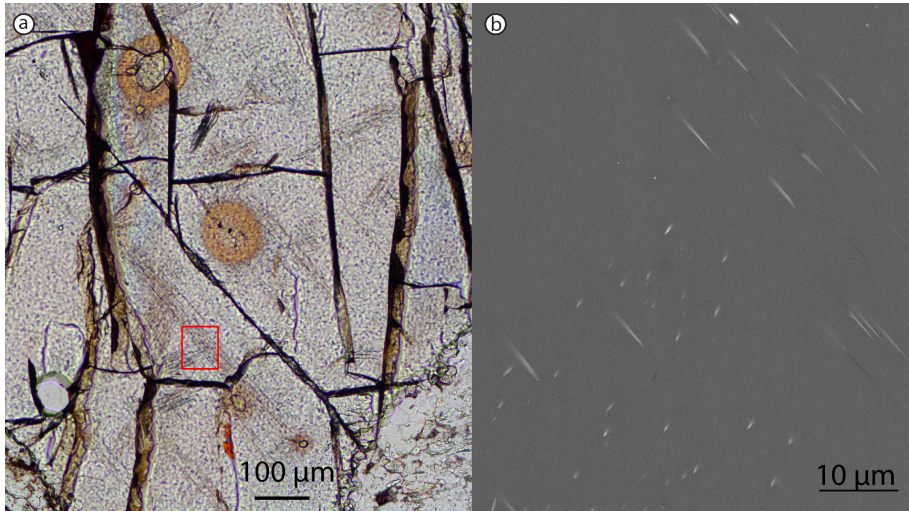
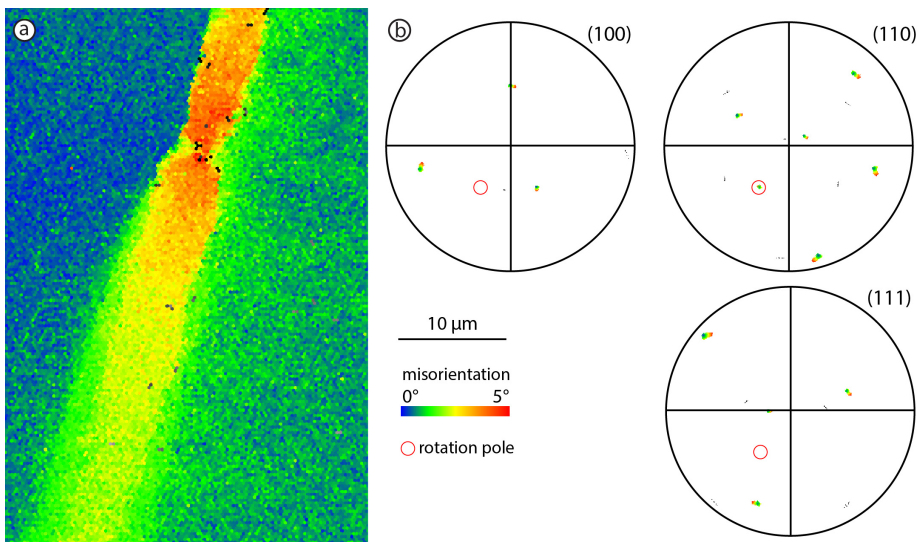


Figure A1: Thin section image in plane polarized light of a garnet crystal with monazite inclusions (with halos) and rutile-exsolution needles. b) BSE-image of the area indicated with the red box.



722 Figure A2: a) Misorientation map-detail for Fig. 6b), with b) pole figure plots for garnet axis
723 with the same ~~color~~colour scheme. The plots reveal a rotation around a (101)-axis, as indicated
724 by the red circle.